Share the Unseen: Sequential Reasoning About Occlusions Using Vehicle-to-Everything Technology

Truls Nyberg, *Member, IEEE*, José Manuel Gaspar Sánchez, Vandana Narri, *Graduate Student Member, IEEE*, Henrik Pettersson, Jonas Mårtensson, *Member, IEEE*, Karl H. Johansson, *Fellow, IEEE*, Martin Törngren, *Senior Member, IEEE*, and Jana Tumova, *Member, IEEE*

***Abstract*— Vehicle-to-everything (V2X) communication holds significant promise for augmenting autonomous driving capabilities. Particularly in dense traffic with occluded areas, V2X can be used to share information about the respective observed areas between traffic participants. In turn, reducing uncertainty about unseen areas can lead to less conservative behaviors while maintaining collision avoidance. This article aims to leverage V2X to improve situation awareness for trajectory planning. We particularly address two challenges. First, the ego vehicle may not always receive up-to-date information. Second, some areas may remain occluded despite receiving information from other participants. In this work, we fuse the received information about the detected free space. We use reachability analysis to compute areas that are guaranteed to be free despite being occluded. This way, we can maintain collision-avoidance guarantees. We demonstrate the benefits of our proposed method both in simulations and physical experiments.**

***Index Terms*— Intelligent vehicles, vehicle-to-everything (V2X), reachability analysis, vehicle safety.**

I. Introduction

AUTONOMOUS vehicles (AVs) must operate safely, ideally guaranteeing collision avoidance even under unpredictable conditions such as occlusions, where visibility is compromised. However, overly conservative driving can significantly impede traffic flow, efficiency, and even safety [1], [2], strongly motivating the investigation of collaborative approaches for connected AVs (CAVs) [3]. Our previous work addressed this problem by developing a method to dynamically assess and minimize areas with possible hidden obstacles based on past observations [4]. This approach enabled us to maintain provable collision avoidance, assuming compliance with traffic regulations, while reducing the conservativeness typically seen in AVs, particularly in time-sensitive scenarios such as intersections.

Building on this foundation, our current work expands the situation awareness of CAVs through the implementation of vehicle-to-everything (V2X) communication. This extension aims to provide AVs with an enhanced understanding of traffic conditions in areas beyond their immediate line of sight, effectively seeing around corners and through obstructions. By integrating V2X communication, we propose augmenting the existing framework for occlusion handling, thereby improving the AVs' decision-making processes in real-time traffic situations.

While V2X communication holds significant potential in improving situational awareness for AVs, it is essential to confront its inherent limitations [5]. For instance, even a well-placed roadside unit (RSU) may still suffer from range limitations, blind spots, and occlusions. In addition, AVs must be robust against the inherent risk of communication delays or packet losses. Our research seeks to address these challenges by developing algorithms that can effectively utilize the available data from V2X communications, without solely relying on instantaneous or lossless communication. This approach is aimed at ensuring that AVs can make safe yet efficient decisions, even in the face of delayed data and sensor occlusions.

Fig. 1 shows an example scenario where a vehicle in blue aims to do a left turn. At time $t = 0$ (top figure), its field of view is occluded by the building. The field of view can be extended if a timely message from the RSU arrives, but the motorcycle is still occluded by the truck. If the message received at time $t = 0$ contains measurement from $t = 0$, at a later time $t = 1$ (bottom figure), the blue vehicle can infer that the checkered area behind the yellow vehicle must still be free because: 1) it had received a message from the RSU showing this area as free previously and 2) none of the vehicles that could have been present in the area occluded by the truck in the top figure could reach the checkered area if they respected assumed rules of the road.

A. Contributions

The presented work is an extension of the method presented in [4]. This work contributes to the field of CAVs as follows:

Received 15 January 2024; revised 17 January 2024 and 28 August 2024; accepted 24 October 2024. Date of publication 28 November 2024; date of current version 26 June 2025. This work was supported in part by the Wallenberg AI, Autonomous Systems and Software Program (WASP) funded by the Knut and Alice Wallenberg Foundation; and in part by Entice (Vinnova) under Project 2022-03000. The work of Karl H. Johansson was supported in part by the Swedish Research Council Distinguished Professor Grant under Grant 2017-01078 and in part by the Knut and Alice Wallenberg Foundation Wallenberg Scholar Grant. Recommended by Associate Editor Y. Chen. *(Truls Nyberg, José Manuel Gaspar Sánchez, and Vandana Narri contributed equally to this work.) (Corresponding author: Truls Nyberg.)*

Truls Nyberg and Vandana Narri are with the KTH Royal Institute of Technology, 100 44 Stockholm, Sweden, also with Digital Futures, 100 44 Stockholm, Sweden, and also with Scania CV AB, 151 87 Södertälje, Sweden (e-mail: trulsny@kth.se; vandana.narri@scania.com).

José Manuel Gaspar Sánchez, Jonas Mårtensson, Karl H. Johansson, Martin Törngren, and Jana Tumova are with the KTH Royal Institute of Technology, 100 44 Stockholm, Sweden, and also with Digital Futures, 100 44 Stockholm, Sweden (e-mail: jmgs@kth.se; jonas1@kth.se; kallej@kth.se; martint@kth.se; tumova@kth.se).

Henrik Pettersson is with Scania CV AB, 151 87 Södertälje, Sweden (e-mail: henrik.x.pettersson@scania.com).

Digital Object Identifier 10.1109/TCST.2024.3499832

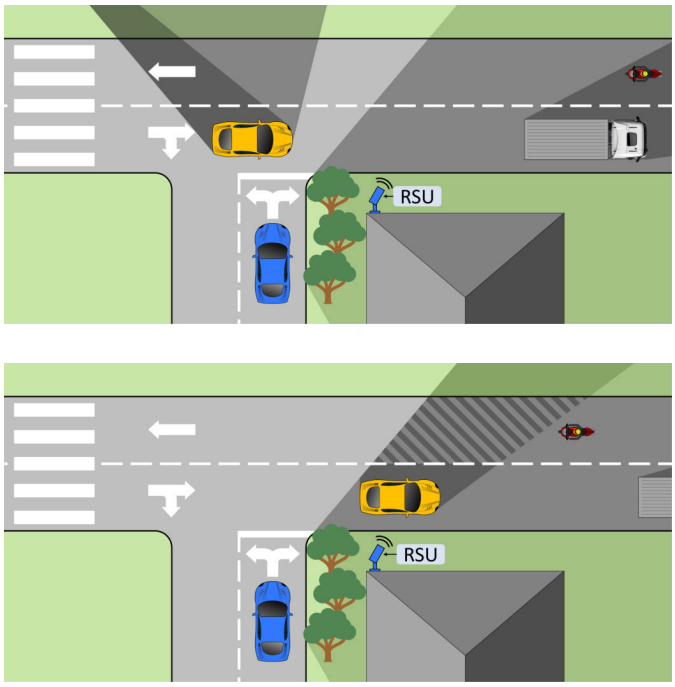

Fig. 1. Top: blue ego vehicle can extend its situation awareness by incorporating the field of view from the RSU about unseen areas, shown in light gray. However, obstacles unseen by both (e.g., the motorcycle in the darker gray area) and possible delays in the communication must be considered as a prerequisite for ensuring safety. Bottom: previous observations from both the ego vehicle and the RSU can be used to conclude where hidden obstacles might be to reduce overdefensive behaviors while maintaining collision avoidance.

1) introducing a robust algorithm for sharing detected free space over V2X communication using reachability to compensate for communication delays while maintaining collision avoidance;
2) integrating the external free space detected into an existing occlusion tracking algorithm [4], minimizing the number of possible hidden obstacles;
3) demonstrating the benefits of the proposed approach both in simulation and physical experiments.

Detailed considerations of performance limitations in the end-to-end cyber–physical systems (e.g., as treated by the safety of the intended functionality (SOTiF) standard [6]) are beyond the scope of this article, as is functional safety [7]. In parallel work [8], we are, however, considering such architectural and failure mode aspects for connected automated vehicles. In [9], we propose a method to accurately estimate free space in the presence of sensor noise and uncertain measurements. In the current work, we rely on this filter to avoid incorrect classification of free space.

B. Outline

The structure of the remainder of this article is outlined as follows. Section II offers a compilation of existing research in this field. Section III details the problem formulation and introduces the necessary preliminaries. Our proposed method is described in Section IV. Section V discusses the simulation setup and the results achieved. This is followed by Section VI, which outlines the real-world experimental setup and its corresponding results. Finally, Section VII concludes this article with a summary and final remarks.

II. Related Work

A. Planning With Hidden Obstacles

The problem of planning under limited visibility has been addressed in multiple works. Chung et al. [10] presented an offline method for path planning under occlusions for indoor robotics using a map of the environment. A more general version of this problem, where the environment is unknown to the robot, is presented in [11]. The approach is based on shrinking the drivable area based on an assumed maximum speed of any hidden obstacle.

Planning under occlusions becomes more complex in a driving environment, where the range of actions of possible occluded vehicles depends on traffic rules. The works in this field can be divided into three main branches: probabilistic methods, interactive approaches, and set-based predictions (SPs).

Probabilistic approaches have been used to compute different metrics indicating the risk of collision based on the current occlusion and road characteristics. Lee et al. [12] use historical speed distribution data per road to compute the probability of collision with an unseen vehicle at an intersection. In [13], random particles generated along unseen lanes are simulated to compute the probability of collision with an unseen vehicle.

The problem of planning under possible hidden obstacles has also been modeled using game theory [14] and partially observable Markov decision processes (POMDPs) [15], [16]. These methods can model interactions between agents, but providing safety guarantees becomes more challenging.

SPs computed with reachability analysis have been used in the field of autonomous driving to overapproximate the future occupancy of all currently visible vehicles and pedestrians, assuming that they follow a set of traffic rules [17], [18], [19]. This approach has also been used to account for possible hidden obstacles by spawning virtual obstacles at the edge of the currently unseen area [20], [21]. A drawback of these methods is that, given that they consider every point outside the current field of view possibly occupied and compute reachability over all of those, they can become quite overconservative, limiting the planning capabilities of the AV.

To reduce the overconservativeness of reachability approaches, some works have focused on reducing the areas where hidden obstacles might be based on previous observations and reachability models. Nager et al. [22] use previous free space observations to track the regions where pedestrians could be. A similar approach is presented in [23] to track possible hidden vehicles following the center lines of lanes. A more general method, without constraining vehicles to specific paths, is presented in [4]. In [24], the model is further developed to track possible velocities of hidden traffic participants, which proves to be particularly beneficial in high-speed scenarios.

B. Vehicle-to-Everything Communication

V2X communication allows the sharing of information between a vehicle and nearby systems, such as other road users or infrastructure elements. Multiple previous works have used V2X communication to share perception information, allowing automated vehicles to increase their knowledge about the environment and improve efficiency or safety.

When sharing perception data, there exists a natural tradeoff between performance and bandwidth. In a so-called *early* collaboration scheme, raw sensor measurements are shared, whereas, in a *late* collaboration scheme, information is instead shared on an object level [25]. Furthermore, when designing a collaborative perception method, challenges such as large data volume, pose errors, and asynchronous communication have to be taken into consideration. These challenges are highlighted and addressed with possible solutions in [26].

In our work, European Telecommunications Standards Institute (ETSI) standards are used when implementing the ITS-G5 access layer and the collaborative perception messages (CPMs) [27], [28]. This communication scheme is well established and can be seen as a late collaboration since the perception information is communicated on an object level. Hasan et al. [29] provide an in-depth discussion of the security standardization for V2X communication. An analysis of the various testing methodologies can be found in [30].

Narri et al. [31], [32] propose a method to fuse information from internal and external sensors to increase the ego vehicle's situational awareness, providing guarantees in the presence of unknown bounded noise on the measurements. This approach is illustrated using communication between two vehicles.

Given the increased knowledge about the environment that V2X communication can provide, multiple works aim to use it to improve traffic flow and increase the safety of AVs [33], [34]. However, many of those studies assume perfect communication, ignoring latency, package losses, and bandwidth limitations. In addition, some also assume full information about the surrounding traffic, proposing methods that are only valid when every traffic participant is connected [35]. Zhang et al. [36] propose a method for incorporating V2X information that accounts for communication delays. Their approach is based on a POMDP planner in which external measurements include a delay factor, which modifies the confidence level of the measurement.

In contrast to previous works, our proposed method aims to take as much benefit as possible from delayed external measurements by computing the areas that could not have been reached in the time of the delay, and must then still be free, given an overapproximation of the reachability model of the unseen obstacles.

III. Problem Formulation

This section first introduces the overall problem settings, including the notation and preliminaries that will be used throughout the rest of this article. Second, it formulates our approach and the key problem that we address.

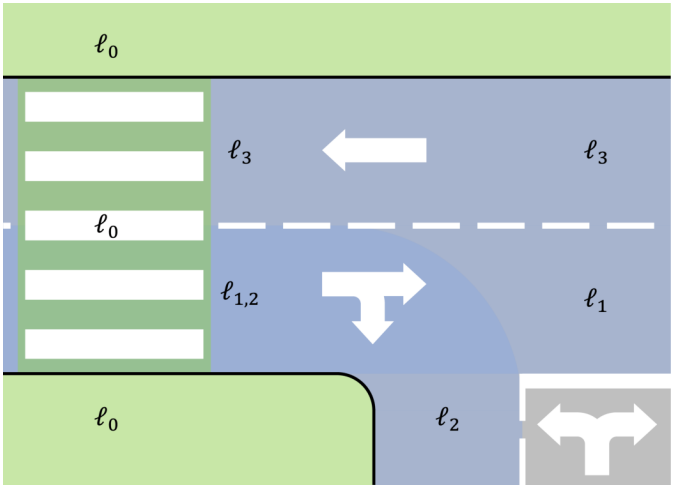

Fig. 2. Representation of the traffic environment as a collection of lanes.

A. Problem Settings

We consider a traffic environment consisting of N lanes, $\ell \in \mathcal{L} = \{\ell_1, \ell_2 \ldots, \ell_N\}$. The road network and static elements are assumed to be available through a map or computed at runtime by another module, which is common in urban areas with high-definition maps or when real-time mapping systems are used. The set $\mathcal{S}^\ell \subset \mathbb{R}^2$ is the set of points in space, which belong to a lane ℓ. To simplify our notation, we also denote walkable areas, such as sidewalks and pedestrian crossings, as lanes. An example of a traffic environment with lanes is shown in Fig. 2. Here, ℓ_0 is a walkable area that may be used by a pedestrian, and the road lanes $\ell_{1:3}$ may be used by cars. The pedestrian crossing is a part of the walkable area ℓ_0 and overlaps with some of the road lanes.

Definition 1 (Valid States on a Lane, $\mathcal{X}^\ell$): The set of valid states on a lane is

$$\mathcal{X}^\ell := \left\{x \in \mathbb{R}^n \mid \text{proj}_{xy}(x) \in \mathcal{S}^\ell\right\}. \tag{1}$$

We denote the state of a traffic participant k, such as a car, bicycle, or pedestrian, at a time t as $x_t^k \in \mathbb{R}^n$. Given the shape $\mathcal{S}^k \subset \mathbb{R}^2$ of the traffic participant, the space it occupies in the xy plane can be computed as

$$\mathcal{O}_t^k = \text{occ}\left(x_t^k, \mathcal{S}^k\right) \tag{2}$$

where the operator occ projects the shape $\mathcal{S}^k$, centered around the xy position of x_t^k.

Definition 2 (Occupied Space): The occupied space $\mathcal{O}_t$ at time t is the union of the space occupied by traffic participants, excluding the ego vehicle.

Definition 3 (Model of a Traffic Participant): We model a traffic participant k as $M^k := \langle f^k, \mathcal{X}^k, \mathcal{U}^k \rangle$, where $\dot{x}^k(t) = f^k(x^k(t), u(t))$ describes the continuous-time dynamic function, $\mathcal{X}^k \subseteq \mathbb{R}^n$ denotes the admissible set of states for the traffic participant k, and $\mathcal{U}^k \subseteq \mathbb{R}^m$ denotes the admissible set of inputs for the traffic participant k.

The admissible state and input sets are determined both by physical constraints and traffic regulations that each participant is expected to follow, such as restrictions on lane usage.

To formally define the feasible and the collision-free trajectory, we introduce the notion of reachability.

Definition 4 (Forward Reachable Set of a Set of States): Given a set of states $\mathcal{X}_t$ at time t, $\mathcal{R}(\mathcal{X}_t, M, \Delta t)$ denotes the set of states reachable from $\mathcal{X}_t$ at time $t + \Delta t$. Formally,

$$\mathcal{R}(\mathcal{X}_t, M, \Delta t) = \left\{ x_t + \int_t^{t+\Delta t} f(x(\tau), u(\tau)) d\tau \;\middle|\; x_t = x(t) \in \mathcal{X}_t,\ x(\tau) \in \mathcal{X},\ u(\tau) \in \mathcal{U}\ \forall \tau \in [t, t+\Delta t] \right\}. \quad (3)$$

Definition 5 (Time-Interval Forward Reachable Set of a Set of States): Given a set of states $\mathcal{X}_t$ and time t, the set of states reachable during a time interval $[t_a, t_b]$ where $t \leq t_a < t_b$ can be computed as

$$\mathcal{R}(\mathcal{X}_t, M, [t_a, t_b]) = \bigcup_{t_a \leq \tau \leq t_b} \mathcal{R}(\mathcal{X}_t, M, \tau - t).$$

With a slight abuse of notation, we use $\mathcal{R}(x_t^k, M^k, \Delta t)$ to denote the reachable set of traffic participant k from state x_t^k computed as $\mathcal{R}(\{x_t^k\}, M^k, \Delta t)$ according to Definition 4. Similarly, we use $\mathcal{R}(x_t^k, M^k, [t_a, t_b])$ to denote the time-interval reachable set $\mathcal{R}(\{x_t^k\}, M^k, [t_a, t_b])$ computed according to Definition 5.

Definition 6 (Feasible Trajectory): A feasible trajectory T^M (under a model M) is a curve in $\mathcal{X} \subseteq \mathbb{R}^n$, where any state $x_{t_b} \in T^M$ is reachable from any state $x_{t_a} \in T^M$ in time $t_b - t_a > 0$, with inputs in $\mathcal{U}$.

Definition 7 (Collision-Free Trajectory): For an ego vehicle in $x_{t_a}^{\text{ego}}$ with a shape $\mathcal{S}^{\text{ego}}$, its trajectory to $x_{t_b}^{\text{ego}}$, denoted T_S, is *collision-free* if $\mathcal{O}_t^{\text{ego}} \cap \mathcal{O}_t = \emptyset$ for all $x_t \in T_S$, $t \in [t_a, t_b]$.

Problem 1 (Planning Problem): Given the state of the ego vehicle x_t^{ego}, a model for the ego vehicle M^{ego}, the state of other traffic participants x_t^k, and models for those other traffic participants M^k, the planning problem is to find the best feasible trajectory (given a cost function) that is guaranteed to be collision-free, T_s.

This is, however, a challenging problem when we consider that some of the traffic participants may be occluded, or outside of the sensors' range, making their states unavailable to the ego vehicle. To represent the detected free space from the ego vehicle's viewpoint, as well as the information about detected free space received via V2X communication from other systems, we introduce the notion of a field of view.

Definition 8 (Field of View, $\mathcal{F}$): A field of view $\mathcal{F}^k \subset \mathbb{R}^2$ of a participant k is defined as the free set of points on the xy plane, which are within direct line of sight from the participant's sensors and within the sensors' range.

Here, we consider the sensor noise to be bounded and assume that the perception system handles this bound. We assume that the field of view is under-approximated, meaning that points are only considered free when sufficient measurements are received to remove all uncertainty. In practice, this can be achieved by applying a safety margin to range measurements, which reduces the impact of sensor noise and eliminates the risk of errors at the boundary of the field of view.

Since we are specifically interested in addressing the issue of possible delays in V2X communication, we also introduce the notion of a time-stamped field of view. We assume that all the systems involved in the V2X communication have access to a shared clock, which is used to time-stamp their respective fields of view. This time-stamp can then be used to compute the delay, which could be caused by the perception system or the communication in the case of external free space, as explained in Section IV.

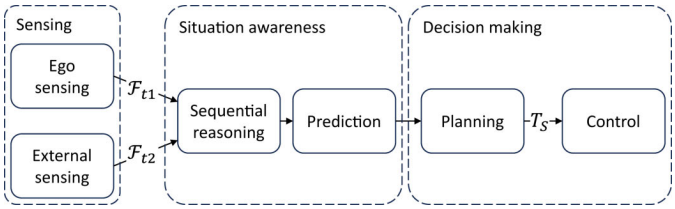

Fig. 3. Representation of the proposed approach. The task is to find a safe trajectory T_s, given multiple fields of view measured at different time steps.

Definition 9 (Time-Stamped Field of View, $\mathcal{F}_t^k$): A time-stamped field of view is defined as a tuple containing a field of view and the time at which it was perceived by the participant k

$$\mathcal{F}_t^k := \langle \mathcal{F}^k, t \rangle. \quad (4)$$

B. Approach

Our approach to tackling the planning problem with a limited field of view is illustrated in Fig. 3. We wish to utilize measurements from both the ego vehicle and other systems that are connected to the ego vehicle via V2X. To that end, an open question is how to fuse the information and sequentially reason about possible hidden obstacles, especially considering possibly delayed measurements arriving unordered. Our objective is to strike a balance in predicting future space occupancy such that we ensure that the prediction is sufficiently conservative and guarantees a collision-free trajectory, without restraining us from finding a plan that is both feasible and close to the optimal trajectory.

Problem 2 (Situation Awareness Problem): Given a model of other traffic participants M^k and a set of time-stamped fields of view of the ego vehicle and other systems, find a minimal overapproximation of the occupied space at the current and future times.

To solve this problem, we make the important assumption that the field of view $\mathcal{F}_t^k$ is detected as free by the agent k and time t is truly free. As explained in Section IV, our approach combines multiple $\mathcal{F}$ from different actors and times, but we do not handle a lack of consistency or uncertainties about the measurements.

IV. Method

This section first addresses the situation awareness problem (see Problem 2) and then presents our overall solution to the planning problem (see Problem 1). In particular, Sections IV-A and IV-B summarize our results from [4]. Section IV-A describes the modeling of possible hidden obstacles. To accurately predict possibly occupied space in the future, Section IV-B describes an algorithm that reasons about

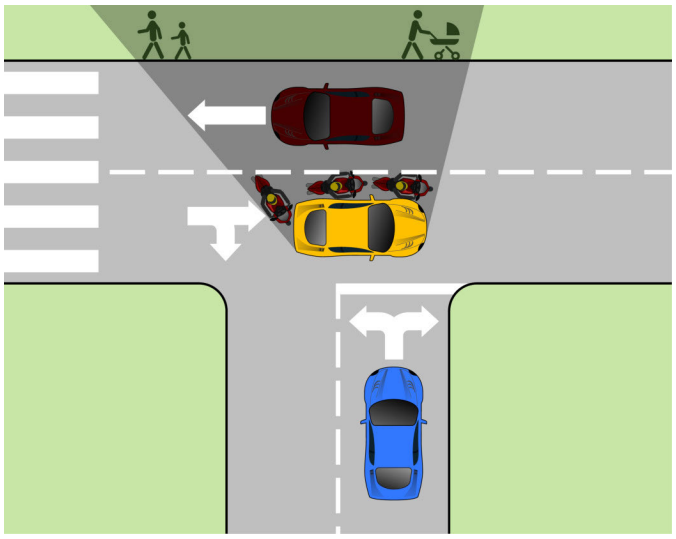

Fig. 4. Ego vehicle is depicted in blue at the bottom. The yellow vehicle in the middle causes an occlusion, illustrated in darker shades. Grayed-out vehicles and pedestrians represent some of the possible hidden obstacles.

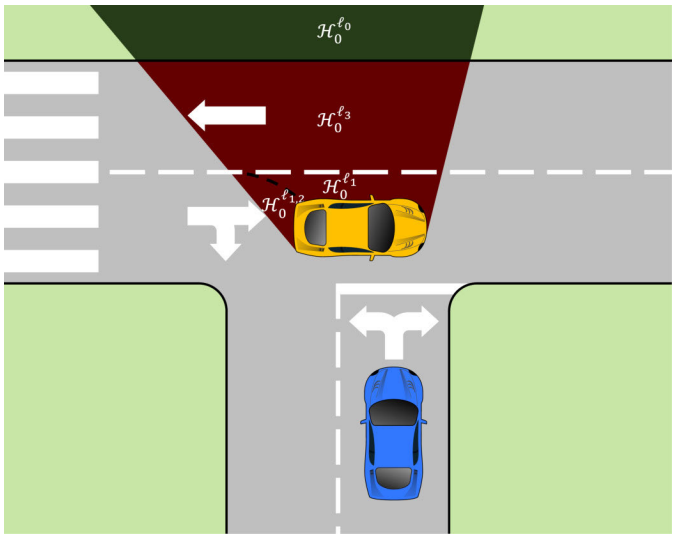

Fig. 5. Illustration of the regions where possible hidden obstacles can be in each lane. States of possible road users are depicted in dark red on the road, and possible pedestrian states are shown in dark green outside the road. All possible hidden obstacles from Fig. 4 are included here.

the possible states of hidden obstacles, given previous free space observations. Here, we assume that the observations are available instantly and ordered in time. However, this generally does not hold when some measurements are received via V2X communication. Section IV-C relaxes these assumptions and describes the algorithm used to reason about possible hidden obstacles when measurements arrive with a delay and can be unordered. Section IV-D finally describes how to incorporate the output of the proposed algorithms into a trajectory planner.

A. Modeling of Possible Hidden Obstacles

Fig. 4 exemplifies a challenging situation, where the ego vehicle, in blue, has a limited field view due to an occlusion caused by another vehicle, in yellow. Computing all possible hidden obstacles that could occupy the area outside of the field of view, with all their possible shapes and states, is a notoriously difficult problem, similar to the polygon containment problem [37]. Some previous works have addressed this problem by finding the worst case placements of hidden obstacles, at the expense of introducing additional assumptions, such as that hidden obstacles follow the center line of the lanes [23]. We instead proposed to model possible hidden obstacles as a set of states $\mathcal{H}$ of a point mass model, filling the possibly occupied region [4]. The benefit of this approach is that any possible hidden obstacle is considered, regardless of its shape or orientation. This also guarantees that no obstacles are missed, however, at the cost of accounting for arbitrarily small obstacles.

In this approach, the set of possible hidden obstacles $\mathcal{H}_t^\ell$ at time t is modeled individually for each lane ℓ. Without loss of generality, we assume that the first measurement takes place at time $t = 0$ with the initial set of states of possible hidden obstacles $\mathcal{H}_0^\ell$ defined as the space within the lane outside of the field of view. An example is illustrated in Fig. 5. Therein, at time $t = 0$, we observe four regions possibly occupied by obstacles: three from the road lanes ℓ_1, ℓ_2, and ℓ_3 and one from the walkable area ℓ_0.

Definition 10 (Initial Set of States of Possible Hidden Obstacles on a Lane:) The set of states of possible hidden obstacles in a lane ℓ at the initial time step $t = 0$ with no prior observations is defined as

$$\mathcal{H}_0^\ell := \left\{x \in \mathcal{X}^\ell \mid \text{proj}_{xy}(x) \notin \mathcal{F}_0\right\}. \tag{5}$$

The main idea behind the prediction is to compute the future possible hidden obstacles' states as the reachable set from $\mathcal{H}_t^\ell$. However, as the shapes of the participants need to be taken into account, it is not sufficient to compute this reachable set using f^k. For instance, the corner of a traffic participant could move faster than the state of the participant if it moves and rotates at the same time. To that end, we propose a new model of hidden obstacles in a lane:

Definition 11 (Model of Hidden Obstacles in a Lane): The model of hidden obstacles in a lane is $M^\ell := \langle f^\ell, \mathcal{X}^\ell, \mathcal{U}^\ell \rangle$, where $\dot{x}_t = f^\ell(x_t, u_t)$ describes the continuous-time dynamic function for the possible hidden obstacles modeled as point masses, $\mathcal{X}^\ell \subseteq \mathbb{R}^2$ denotes the admissible set of states at the lane ℓ, and $\mathcal{U}^\ell \subseteq \mathbb{R}^n$ denotes the admissible set of inputs at the lane ℓ. We require that for all t

$$\text{occ}\big(\mathcal{R}\big(x_t^k, M^k, t\big), \mathcal{S}^k\big) \subseteq \text{occ}\big(\mathcal{R}\big(\mathcal{H}^\ell, M^\ell, t\big), \mathbf{0}\big) \tag{6}$$

for all possible shapes $\mathcal{S}^k$ of any possible hidden obstacle k. The symbol $\mathbf{0}$ represents a point at the origin.

As an example, $f^\ell(x, u)(t) = \{x + ut \in \mathbb{R}^2 \mid u \in S^1\}$ where S^1 is a unit circle would be a suitable representation of how the states of possibly hidden pedestrians may evolve on a walkable area. For a road lane f^ℓ, a suitable function may include other reasonable constraints imposed on vehicles on the lanes, such as that they have to move within the direction of the lane and they have to obey a speed limit.

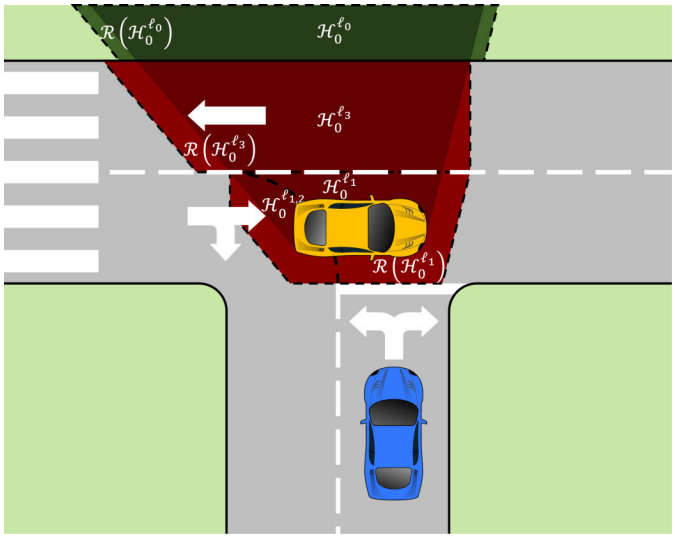

Fig. 6. Reachable sets of the regions of possible hidden obstacles from Fig. 5 are illustrated within the dashed area.

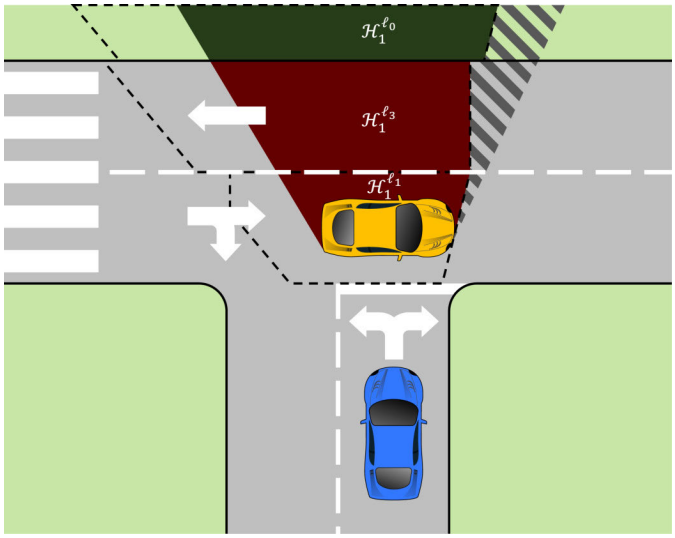

Fig. 7. Reachable sets of the regions of possible hidden obstacles from the previous time step are shown within the dashed black lines. The region toward the top right from the yellow vehicle hashed in gray is concluded to not contain any possible hidden obstacles even though it is outside $\mathcal{F}_{t_1}$ since it is not within the reachable set from the previous time step.

When modeling the reachable set, it is important to make sure that it is both: 1) an overapproximation of the true reachable set of states and 2) possible to compute in an efficient way. In this work, we only consider the positional states and assume that the true reachable set of hidden traffic participants can be overapproximated by the reachable set of a constrained single-integrator system. This can efficiently be computed using a Minkowski sum, as done in [4] and [24].

B. Prediction of Possibly Hidden Obstacles With Ordered Measurements

Let us assume that measurements are taken and instantly available at times $t_0 = 0, t_1, t_2, \ldots$. The set of possible hidden obstacles at time t_j in lane ℓ is computed based on the reachable set of the previous possible hidden obstacles $\mathcal{H}^{\ell}_{j-1}$ and the current field of view $\mathcal{F}_{t_j}$.

Definition 12 (States of Possible Hidden Obstacles): The states of possible hidden obstacles at time t_j in a lane ℓ are

$$\mathcal{H}^{\ell}_{t_j} = \left\{ x \in \mathcal{R}\left(\mathcal{H}^{\ell}_{t_{j-1}}, M^{\ell}, \Delta t\right) \mid \text{proj}_{\text{xy}}(x) \notin \mathcal{F}_{t_j} \right\} \quad (7)$$

where $\Delta t = t_j - t_{j-1}$.

Fig. 6 shows an example of the reachable set $\mathcal{R}(\mathcal{H}^{\ell}_0, M^{\ell}, \Delta t)$ where $\mathcal{H}^{\ell}_0$ is the set from Fig. 5. In this case, the model M^{ℓ}, particularly the function f^{ℓ}, assumes that traffic in lanes ℓ_1–ℓ_3 can move forward and sideways within the lane up to a maximum speed, but not backward. In contrast, pedestrians in the walkable area ℓ_0 are assumed to be able to move in any direction at a lower maximum speed. Fig. 7 illustrates what the sets of possible hidden obstacles look like at time t_1. Once the yellow vehicle has moved forward, the states within $\mathcal{R}(\mathcal{H}^{\ell}_0, M^{\ell}, \Delta t)$ that are outside of the field of view $\mathcal{F}_{t_1}$ remain considered the states of possibly hidden obstacles at time t_1.

Lemma 1: Any possible hidden obstacle in a lane ℓ at time t_j must have a state $x \in \mathcal{H}^{\ell}_{t_j}$.

Proof: From Definition 8 of $\mathcal{F}$ and Definition 4 of $\mathcal{R}^{\ell}$, we conclude the following.

1) The state of a possible hidden obstacle must be in the reachable set of all possible hidden obstacle states from the previous time step, i.e., $x \in \mathcal{R}^{\ell}(\mathcal{H}^{\ell}_{t_{j-1}}, M^{\ell}, \Delta t)$.
2) The projection of a possible hidden obstacle state can not be in our field of view, i.e., $x \in \mathcal{X} \mid \text{proj}_{\text{xy}}(x) \notin \mathcal{F}_{t_j}$.

Therefore, the set of all of states of possible hidden obstacles at the current time t_j in a lane ℓ must be all states such that (1) and (2) hold, i.e., $\{x \in \mathcal{R}^{\ell}(\mathcal{H}^{\ell}_{t_{j-1}}, M^{\ell}, \Delta t) \mid \text{proj}_{\text{xy}}(x) \notin \mathcal{F}_{t_j}\}$. ■

C. Tracking of Possible Hidden Obstacles With Unordered Measurements

Up until this point, we have assumed that sensor measurements are available in the order in which they are taken. When incorporating external measurements through V2X communication, this assumption is no longer valid, i.e., the external measurements could get lost, they could arrive in a different order than they were taken, and specifically, older external measurements could arrive after a newer internal measurement taken by the ego vehicle. Fig. 8 depicts a scenario where an external sensor shares its field of view with the ego vehicle, shown in blue at the bottom.

In this section, we present an approach to incorporate sensor measurements asynchronously. We do not distinguish between the external and the internal measurements, but we assume that each sensor measurement is time-stamped with a common clock shared by the ego vehicle and the external sensors, allowing us to compute how old a measurement is after receiving it. This approach, even though exemplified with an external sensor setup, could also be used when merging multiple sensor measurements from the same system that could be subject to delays in their processing.

Table I summarizes the notation for measurement time stamps used in the following definitions.

Let $\mathcal{H}^{\ell}_0$ be defined as in Definition 10 considering the field of view of the ego vehicle only.

Definition 13 (States of Possible Hidden Obstacles Given Only One Measurement): Similar to Definition 10, we define

TABLE I
NOTATION USED FOR DIFFERENT TIMES

t_{meas}	when the newest available measurement was taken
t_{prev}	when the previously latest available measurement was taken
t_{latest}	$\max(t_{\text{prev}}, t_{\text{meas}})$
t_{earlier}	$\min(t_{\text{prev}}, t_{\text{meas}})$

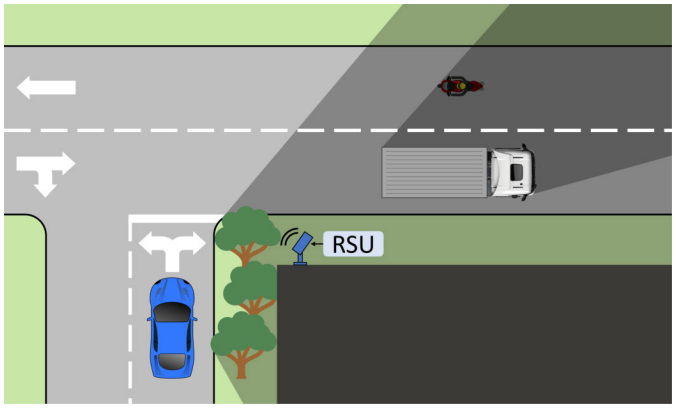

Fig. 8. Light-shaded area represents the region within the field of view of the external sensor but outside of the field of view of the ego vehicle. The dark-shaded area represents the region outside of the field of view of both; within this region, there is a hidden motorcycle, which might have already moved into the field of view of the external sensor by the time the ego vehicle receives the message from the external sensor that does not include it.

the set of possible hidden obstacles' states at t_{meas} given only the time-stamped field of view $\mathcal{F}^k_{t_{\text{meas}}}$ from agent k as

$$\mathcal{H}^{\ell,k}_{t_{\text{meas}}} = \left\{x \in \mathcal{X}^\ell \mid \text{proj}_{\text{xy}}(x) \notin \mathcal{F}^k_{t_{\text{meas}}}\right\}. \tag{8}$$

Definition 14 (States of Possible Hidden Obstacles Given Asynchronous Measurements):

Assume that the latest previous measurement that arrived before time t was taken at time t_{prev}. Assume that a new measurement arrives at time t that was taken at time t_{meas} by participant k. Note that t_{meas} may be smaller, equal, or larger than t_{prev}. The set of possible hidden obstacles' states is then defined as

$$\mathcal{H}^\ell_{t_{\text{latest}}} = \begin{cases} \mathcal{R}\left(\mathcal{H}^\ell_{t_{\text{prev}}}, M^\ell, \Delta t\right) \cap \mathcal{H}^{\ell,k}_{t_{\text{meas}}}, & t_{\text{prev}} \leq t_{\text{meas}} \\ \mathcal{R}\left(\mathcal{H}^{\ell,k}_{t_{\text{meas}}}, M^\ell, \Delta t\right) \cap \mathcal{H}^\ell_{t_{\text{prev}}}, & t_{\text{prev}} > t_{\text{meas}} \end{cases} \tag{9}$$

where $\Delta t = t_{\text{latest}} - t_{\text{earlier}}$.

Lemma 2: Any possible hidden obstacle in a lane ℓ at time t_{latest} must have a state $x \in \mathcal{H}^\ell_{t_{\text{latest}}}$.

Proof: There are two cases in Definition 14.

1) $t_{\text{prev}} \leq t_{\text{meas}}$*:* In this case, at time $t_{\text{latest}} = t_{\text{meas}}$, we conclude that the following holds.
   a) The state of any possible hidden obstacle must be in the reachable set of all possible hidden obstacle states from t_{prev}, i.e., $x \in \mathcal{R}(\mathcal{H}^\ell_{\text{prev}}, M^\ell, \Delta t)$.
   b) The projection of any possible hidden obstacle state can not be in the field of view of the measurement, i.e., $x \in \mathcal{H}^{\ell,k}_{t_{\text{meas}}} = \mathcal{X}^\ell \mid \text{proj}_{\text{xy}}(x) \notin \mathcal{F}_{\text{meas}}$.

   Therefore, the set of all states of possible hidden obstacles at time t must be such that a) and b) hold, i.e., $\{x \in \mathcal{R}(\mathcal{H}^\ell_{\text{prev}}, M^\ell, \Delta t) \mid x \in \mathcal{H}^{\ell,k}_{t_{\text{meas}}} = \{x \in \mathcal{R}(\mathcal{H}^\ell_{t_{\text{prev}}}, M^\ell, \Delta t) \cap \mathcal{H}^{\ell,k}_{t_{\text{meas}}}\}$.
2) $t_{meas} \leq t_{prev}$*:* In this case, at time $t = t_{\text{prev}}$, we conclude the following.

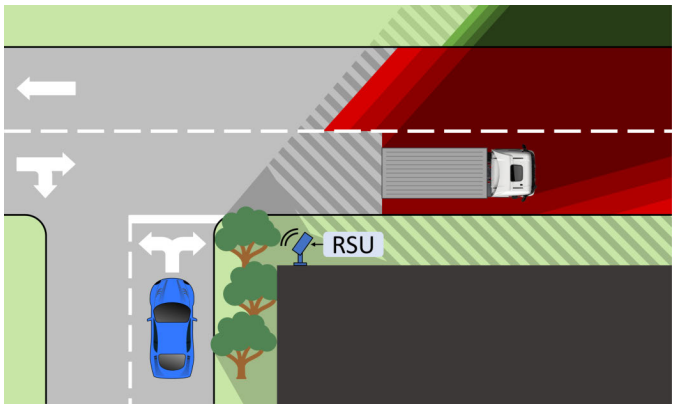

Fig. 9. Illustration of how the blue vehicle with our method can utilize a field of view measurement that arrives three time steps later than the measurement time.

   a) That the state of any possible hidden obstacle must belong to the reachable set of the states which projection was outside the external field of view at the time of the measurement, i.e., $x \in \mathcal{R}(\{x \in \mathcal{X}^\ell \mid \text{proj}_{\text{xy}}(x) \notin \mathcal{F}_{\text{meas}}\}, M^\ell, \Delta t) = \mathcal{R}(\mathcal{H}^{\ell,k}_{t_{\text{meas}}}, M^\ell, \Delta t)$.
   b) The state of any possible hidden obstacle must belong to the previous set of possible hidden obstacles, i.e., $x \in \mathcal{H}^\ell_{\text{prev}}$.

   Therefore, the set of all states of possible hidden obstacles at time t must be such that a) and b) hold, i.e., $\{x \in \mathcal{R}(\mathcal{H}^{\ell,k}_{t_{\text{meas}}}, M^\ell, \Delta t) \mid x \in \mathcal{H}^\ell_{\text{prev}}\} = \{x \in \mathcal{R}(\mathcal{H}^{\ell,k}_{t_{\text{meas}}}, M^\ell, \Delta t) \cap \mathcal{H}^\ell_{t_{\text{prev}}}\}$.

■

Fig. 9 shows an example of the proposed method. The ego vehicle has been tracking possible hidden obstacles with its sensors up to the time of its last sensor measurement t_{prev}. Then, the ego vehicle receives the field of view from the external sensor $\mathcal{F}^k_{\text{meas}}$ with a delay of three time units with respect to its latest sensor measurement, i.e., $t_{\text{meas}} = t - 3$. We first compute the set of possible hidden obstacles outside the field of view at the time of the sensor measurement, $\mathcal{H}^{\ell,k}_{t_{\text{meas}}} = \{x \in \mathcal{X}^\ell \mid \text{proj}_{\text{xy}}(x) \notin \mathcal{F}^k_{t_{\text{meas}}}\}$. To compensate for the delay, the reachable set of those possible hidden obstacles, $\mathcal{R}(\mathcal{H}^{\ell,k}_{t_{\text{meas}}}, M^\ell, \Delta t)$, is computed up to the time t_{prev}. After incorporating this set, hidden obstacles in the dashed area are removed.

Algorithm 1 presents the method used to compute the states of possible hidden obstacles. The algorithm takes as input the latest available set of states of possible hidden obstacles for each lane, $\mathcal{H}^{\mathcal{L}}_{t_{\text{prev}}}$, the time of the most recent measurement, t_{prev}, and the field of view of the new measurement, $\mathcal{F}_{t_{\text{meas}}}$, and the time when the new measurement was produced, t_{meas}. As output, it provides the updated set of possible hidden obstacles per lane, $\mathcal{H}^{\mathcal{L}}_{t_{\text{latest}}}$, and the time of the latest sensor measurement, t_{latest}. The algorithm has three cases: initialization, update with a sensor measurement newer than the previous latest measurement available, and update with a sensor measurement older than the previous latest measurement available.

D. Planning Considering Possible Hidden Obstacles

After computing the possible locations of hidden obstacles based on previous observations, as detailed in

Algorithm 1 Computing States of Possible Hidden Obstacles

INPUT: $\mathcal{H}^{\mathcal{L}}_{t_{\text{prev}}}, t_{\text{prev}}, \mathcal{F}^{k}_{t_{\text{meas}}}, t_{\text{meas}}, \mathcal{L}$
OUTPUT: $\mathcal{H}^{\mathcal{L}}_{t_{\text{latest}}}, t_{\text{latest}}$

$\mathring{\mathcal{H}}^{\ell,k}_{t_{\text{meas}}} = \{x \in \mathcal{X}^{\ell} \mid \text{proj}_{\text{xy}}(x) \notin \mathcal{F}^{k}_{t_{\text{meas}}}\}$
$\Delta t = |t_{\text{meas}} - t_{\text{prev}}|$
foreach $\ell \in \mathcal{L}$
  if $t_{\text{prev}} = 0$
    $t_{\text{latest}} \leftarrow t_{\text{meas}}$
    $\mathcal{H}^{\ell}_{t_{\text{latest}}} \leftarrow \mathring{\mathcal{H}}^{\ell,k}_{t_{\text{meas}}}$
  else if $t_{\text{prev}} \leq t_{\text{meas}}$
    $t_{\text{latest}} \leftarrow t_{\text{meas}}$
    $\mathcal{H}^{\ell}_{t_{\text{latest}}} \leftarrow \mathcal{R}(\mathcal{H}^{\ell}_{t_{\text{prev}}}, M^{\ell}, \Delta t) \cap \mathring{\mathcal{H}}^{\ell,k}_{t_{\text{meas}}}$
  else
    $t_{\text{latest}} \leftarrow t_{\text{prev}}$
    $\mathcal{H}^{\ell}_{t_{\text{latest}}} \leftarrow \mathcal{R}(\mathring{\mathcal{H}}^{\ell,k}_{t_{\text{meas}}}, M^{\ell}, \Delta t) \cap \mathcal{H}^{\ell}_{t_{\text{prev}}}$
$\mathcal{H}^{\mathcal{L}}_{t_{\text{latest}}} \leftarrow \langle \mathcal{H}^{\ell_1}_{t_{\text{latest}}}, \mathcal{H}^{\ell_2}_{t_{\text{latest}}}, \ldots, \mathcal{H}^{\ell_N}_{t} \rangle$
return $\mathcal{H}^{\mathcal{L}}_{t_{\text{latest}}}, t_{\text{latest}}$

Sections IV-B and IV-C, we can now predict their future states. These predictions can be generated in various ways, as shown in [38] and [39]. In our case, we apply the same reachability analysis used for reasoning to forecast the potential future positions of hidden obstacles.

Algorithm 2 shows an example of how to incorporate possible hidden obstacles into a sampling-based planner. The inputs to the algorithm are the set of possible hidden obstacles per lane, $\mathcal{H}^{\mathcal{L}}_{t_{\text{prev}}}$; the time of the latest measurement used to compute those possible hidden obstacles, t_{prev}; the state of the ego vehicle, $x^{\text{ego}}_{t_{\text{latest}}}$; the current time, t_{latest}; the prediction horizon, N; the time step length, Δt; and the set of lanes, $\mathcal{L}$. The output of the algorithm is a trajectory T, which is guaranteed to be collision-free under the assumption that other traffic participants stay within the reachable set of valid states within their lanes.

The algorithm computes the reachable sets of possible hidden obstacles per lane for the N time intervals to guarantee that the planned trajectory is collision-free in between each two consecutive time steps. Afterward, a set of candidate trajectories, $\mathcal{T}$, is generated, and the set of safe trajectories $\mathcal{T}_{\mathcal{S}} \subset \mathcal{T}$ is computed. Finally, the best trajectory, T, is selected based on a cost function.

V. Simulated Experiments

These experiments aim to demonstrate how tracking possible hidden obstacles over time, using a combination of ego vehicle perception augmented with perception from external units, can improve the performance of AVs while maintaining collision avoidance. We compare our proposed approach against different baseline alternatives in a simulated intersection, initially presented in [20] and later used in [4]. This scenario represents one of the most common and challenging driving situations: a left turn where the ego vehicle has to yield to others. The code to run the presented experiments and results from the simulations are available on GitHub.[1]

[1]https://github.com/KTH-RPL-Planiacs/share-the-unseen

Algorithm 2 Planning With Possible Hidden Obstacles

INPUT: $\mathcal{H}^{\mathcal{L}}_{t_{\text{latest}}}, x^{\text{ego}}_{t_{\text{latest}}}, t_{\text{latest}}, N, \Delta t, \mathcal{L}$
OUTPUT: T

foreach $\mathcal{H}^{\ell}_{t_{\text{latest}}} \in \mathcal{H}^{\mathcal{L}}_{t_{\text{latest}}}$
  foreach $i \in 1$ **to** N
    $t_a \leftarrow t_{\text{latest}} + (i-1)\Delta t$
    $t_b \leftarrow t_{\text{latest}} + i\Delta t$
    $\mathcal{O}^{\ell}_{[t_a,t_b]} \leftarrow occ(\mathcal{R}(\mathcal{H}^{\ell}_{t_{\text{latest}}}, M^{\ell}, [t_a, t_b]), \mathbf{0})$
    $\mathcal{O}_{[t_a,t_b]} \leftarrow \mathcal{O}_{[t_a,t_b]} \cup \mathcal{O}^{\ell}_{[t_a,t_b]}$
$\mathcal{T} \leftarrow \text{generateTrajectories}(x^{\text{ego}}_{t_{\text{latest}}})$
$\mathcal{T}_s \leftarrow \text{getSafeTrajectories}(\mathcal{T}, \langle \mathcal{O}_{[t_{\text{latest}},t_{\text{latest}}+\Delta t]}, \ldots, \mathcal{O}_{[t_a,t_b]} \rangle)$
$T \leftarrow \text{getBestTrajectory}(\mathcal{T}_s)$
return T

A. Experiments Setup

1) Baselines: In this work, we propose a method that considers possible hidden traffic participants by: 1) recursively computing the reachable set of those possible hidden traffic participants to track potential locations and 2) incorporating information from external sensors to enhance situational awareness, compensating for possible delays using the same reachability models. For this reason, we compare with the following three baselines.

1) *SPs:* The methods presented in [20] and [21], where possible hidden obstacles are considered anywhere outside the current field of view, i.e., there is no tracking or sharing of external information.
2) *Sequential Reasoning (SR):* Our previous method, presented in [4], where possible hidden obstacles are tracked using reachability as in this work, but no external information is included.
3) *SPs With External Information (SP-E):* To the best of our knowledge, this approach has not been directly proposed for tracking possible hidden obstacles, but it is a natural extension of the SP methods. In this approach, free space from external units is combined with the ego vehicle's detected free space similar to our proposed approach but without the sequential tracking. As previously described, delays in communication are also compensated for using reachability analysis.

2) Scenario: We use the road network from Fürstenfeldbruck presented in [20] and later used in [4], where an AV has to plan a left turn in an intersection, while it has to yield to others. The field of view of the ego vehicle is limited both by a building and by a moving vehicle traversing the intersection. The scenario has been adapted by adding an external sensor close to the intersection used for the SP-E baseline and our proposed SR with external information (SR-E).

3) Implementation: The scenario is simulated and visualized using the CommonRoad toolbox [40], and the collision checking is done with CommonRoad's drivability checker [41]. The fields of view are computed by ray tracing from the sensors' positions. The valid states on a lane are obtained from the lane's perimeter on CommonRoad's map and 120% of the lane's speed limit. All set operations are

computed using the Python package Shapely [42]. Similar to [4], we use a single integrator as the dynamical model for possible hidden obstacles to generate overapproximate predictions and reduce computational complexity. The input velocity is limited to be along the lane's driving direction and between zero and the lane's maximum assumed velocity. The set of states is stored as Shapely (2-D) Polygons, where the Minkowski sum is computed using the buffer function with the maximum velocity as input.

4) Visualization: Scenarios are presented with snapshots at different time steps. The figures show the ego vehicle in blue following a black line depicting its planned trajectory, other vehicles in yellow, and static obstacles in gray. The ego vehicle's field of view is shown in light blue, and the latest received external sensor view is shown in light green, i.e., the external sensor view is shown delayed based on the communication latency. Regions with possible obstacles are shown in two tones of red, with the lighter one highlighting the areas that, even though perceived as free by the external sensor, are considered possibly occupied due to the possible movement of hidden obstacles during the delay in the communication. Cardinal directions are used when referring to lanes and vehicle routes. The ego vehicle is assumed to always be arriving from the south in the figures.

B. Results

Fig. 10(a)–(c) shows the results for SPs. In Fig. 10(a), the ego vehicle's path through the intersection is blocked both by the yellow vehicle coming from the left and the prediction of possible hidden obstacles coming from the east. In Fig. 10(b) and (c), the yellow vehicle has already passed the intersection, but the ego vehicle is still waiting due to some possible hidden obstacles coming from the east.

Fig. 10(d)–(f) shows the same scenario using SP-E. Fig. 10(d) shows in red the set of possible hidden obstacles when the ego vehicle is still approaching the intersection. Despite the communication delay (compensated by the areas marked in light red), large sections of the lanes are deduced free of possible hidden obstacles, thanks to the external sensor. However, Fig. 10(e) and (f) shows that for this scenario and external sensor position, there are no positive effects on the motion planning of the ego vehicle since the lane coming from the right is simultaneously occluded to both sensors.

Fig. 10(g)–(i) shows the results for the same scenario using the SR approach without external information. At the time $t = 1.5$ s, in Fig. 10(g), the possibility of a hidden obstacle traveling has already been discarded since the hidden vehicle would have had to be traveling backward in the lane. At the time $t = 2.5$ s, in Fig. 10, the algorithm has ruled out the option of a hidden obstacle on the lane coming from the east behind the yellow vehicle. Despite that, the ego vehicle is still planning to stop due to the occlusions caused by the building. Once the ego vehicle gets close enough to the intersection to remove the occlusion caused by the building, it is able to plan a trajectory through the intersection, as shown in Fig. 10(i).

Fig. 10(j)–(l) shows the results when using our proposed SR-E. At the time $t = 1.5$ s, in Fig. 10(j), the area with possible hidden obstacles is considerably smaller compared to baselines. At the time $t = 2.5$ s, in Fig. 10(k), the ego vehicle is already able to plan a safe trajectory through the intersection due to the combined tracking of possible hidden obstacles and the inclusion of external information.

Fig. 11 shows the velocity profiles achieved by the ego vehicle with each of the baselines and our proposed method. As mentioned earlier, SP and SP-E achieve the same performance, forcing the ego vehicle to get to a full stop due to possible hidden obstacles behind the yellow car. SR improves the performance by ruling out the option of hidden obstacles behind the yellow vehicle traversing toward the intersection. However, it still causes a speed reduction due to the occlusion of the building. In contrast, with our proposed method, the vehicle traverses the intersection while maintaining its target speed and ensuring collision avoidance.

VI. Real-World Experiments

In this section, we demonstrate results from real-world experiments. The experiments were carried out at Scania's test track using three trucks: one as the ego-vehicle, one acting as an RSU, and one creating an occlusion in the ego-vehicle's field of view. We start this section with a description of the scenario considered for the real-world experiments. This is followed by a description of the hardware setup and implementation. Finally, we conclude this section with the results and discussion.

A. Scenario Setup

To demonstrate the problem and the proposed method, we set up a scenario in a T-junction with limited visibility. The scenario consists of a tractor with an attached semitrailer acting as the ego vehicle, a moving construction truck causing an occlusion, and a parked tractor acting as an RSU, as presented in Figs. 12 and 13.

The goal for the ego vehicle in this scenario is to make a right turn and enter the main road safely. Since traffic on the main road has priority, the ego vehicle must yield to vehicles coming from the left. Also, since the ego vehicle is a tractor with an attached semitrailer, its turning radius is limited compared to a passenger car. As a result, the ego vehicle will briefly need to enter the opposing lane to make the turn, requiring it to yield to vehicles approaching from the right as well.

The ego vehicle is equipped with a sensor suite providing a field of view. It is also receiving time-stamped field-of-view measurements of the intersection from the RSU. Using the received measurements and its own field of view, the ego vehicle must find a feasible, collision-free trajectory to enter the main road. However, as shown in Fig. 13, the opposing lane (to the right) will, at some point, partly be occluded from both the ego vehicle and the RSU. The ego vehicle must, therefore, be able to reason about whether or not an object may be hidden in the jointly occluded region behind the construction truck.

B. Hardware and Implementation

The method proposed in Section IV was implemented and tested on the Traton Autonomous Platform, deployed

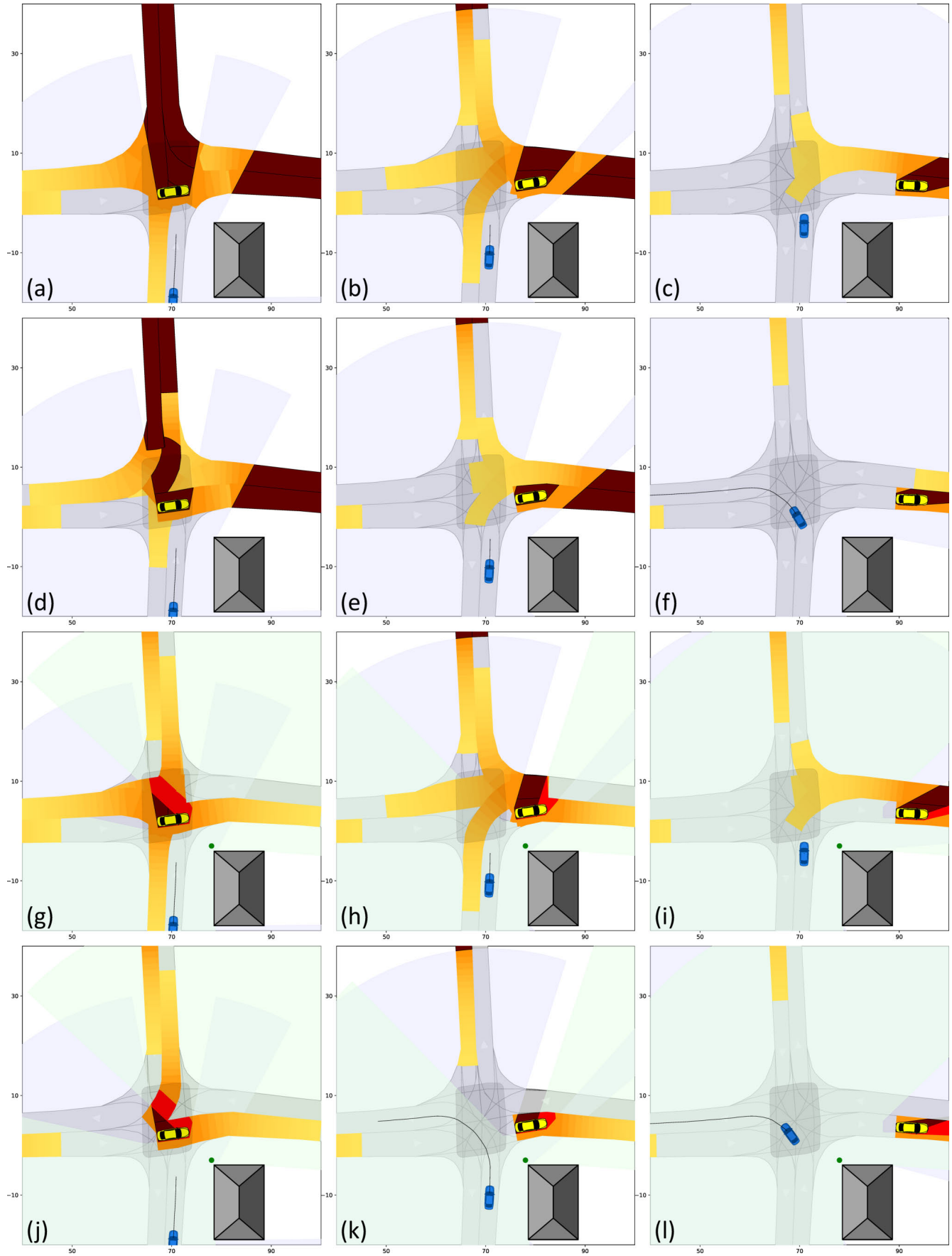

Fig. 10. Simulation results comparing a scenario executed with the four described methods, visualized at three chosen time steps. The rows correspond to the methods SP, SR, SP-E, and our SR-E, respectively, and the columns to time stamps 1.5, 2.5, and, 4.0 s after the scenario is initialized. The rows correspond to the methods, and the columns to the timestamps. For example, (e) shows the result with method SR at timestamp 2.5 seconds, as stated in the caption.

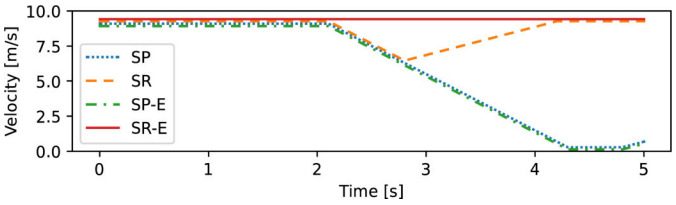

Fig. 11. Achieved velocity over time when using the four methods compared.

Fig. 12. Ego vehicle (the tractor with an attached semitrailer) waits for the construction truck approaching from its left to pass. To the right, another tractor is parked, acting as an RSU.

Fig. 13. Construction truck has passed the intersection and is currently occluding the opposing lane from both the ego vehicle and the RSU. For the ego vehicle to safely enter the intersection, it must make sure that no vehicle is approaching from either side since it will briefly have to occupy the opposing lane to make the right-hand turn.

in Scania's autonomous prototype vehicles. These vehicles leverage several technologies for positioning and perception, including a Real Time Kinematic Global Positioning System (RTK-GPS), a fused occupancy map from six LiDAR sensors, a V2X module for communicating CPMs, and an HD map of the environment detailing lane structures.

The platform fuses LiDAR measurements to generate a time-stamped occupancy grid map, which serves as the vehicle's field of view. Communication between internal applications is managed via the data distribution service (DDS), facilitating real-time data exchange. Externally, the vehicles communicate with each other using V2X, enabled by onboard Commsignia ITS-OB4 units. These units implement the ITS-G5 access layer as specified by the ETSI [28], providing an embedded solution for vehicular communication. In this work, we utilize standardized CPMs that include the *Free Space Addendum* container [27]. The messages are transmitted at a rate of 10 Hz over dedicated short-range communication (DSRC), built on the ITS-G5 standard. Similar to Wi-Fi, ITS-G5 is a European standard for vehicular communication based on IEEE 802.11x.

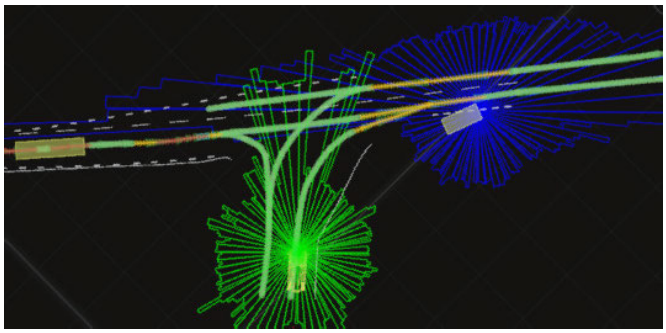

Fig. 14. Initial pose where the ego vehicle waits for the construction truck from the left to pass. Another truck is acting as an RSU and communicating its field of view. Most parts of the lanes are marked green since they are detected free, either by the ego vehicle or the RSU. Some parts close to the RSU are marked yellow since they were communicated to be free in an older message, yet our algorithm concludes that no obstacle can currently be there.

To integrate the method in Section IV with the existing system, some adjustments to the implementation in Section V were made. For instance, the set of valid states was restricted to be positioned along the centerlines of lanes. Also, instead of representing the set $\mathcal{F}_t$ as time-stamped polygons, occupancy grid maps were used internally. However, when transmitting $\mathcal{F}_t$, it had to be converted into no more than 128 free space polygons with a maximum of 16 vertices each to comply with the standard. Also, the maximum size of the CPM is restricted to 1343 B in total [43]. This means that the available payload for the free space addendum depends on what is being communicated in the CPM [5].

In our implementation, $\mathcal{F}_t$ was converted into 64 polygons, each with up to eight vertices. The polygon vertices were created by ray tracing in the occupancy grid map, outward from the vehicle's position. Due to the restriction in payload, the polygons were sent in two consecutive CPMs. When receiving these free space polygons, they were then again converted back to an occupancy grid map to fit the internal representation.

C. Results

Figs. 14 and 15 show the internal representation of the state of the environment from the ego vehicle's perspective. In Figs. 14 and 15, white solid and dashed lines represent the lanes of the scenario, and the green arrows represent the direction of the lanes.

$\mathcal{F}_t$ from the ego vehicle is represented by green polygons. Similarly, $\mathcal{F}_t$ from the RSU is represented by blue polygons. The green lines in the lane center represent regions that are visible and not occupied by another road user. The red lines represent regions that are occluded and might be occupied by some other road user. The yellow lines represent occluded regions that are concluded to be free due to the SR of our algorithm.

Fig. 14 shows the internal representation of the scenario at the initial time, as shown in the photograph in Fig. 12. As earlier described, the RSU sends its field of view in two messages due to the limitations of the CPM standard. In Fig. 14, the ego vehicle has just processed a CPM message with free space to the right of the RSU and marked those lanes

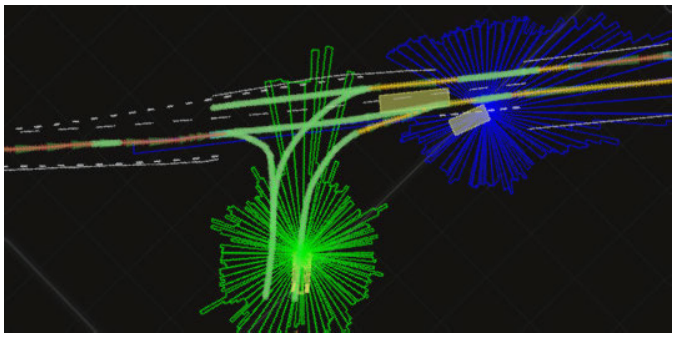

Fig. 15. Construction truck has passed and is now occluding the opposite lane from the ego vehicle and the RSU. Thanks to SR about possible hidden obstacles, our algorithm concludes that this area is still free from obstacles.

free (shown in green). Previously, it has received a message with the RSU's remaining field of view. Thanks to the SR, this area (shown in yellow) can be concluded to be free even though it is not currently observed.

Fig. 15 shows the internal representation of the scenario at a later time, as shown in the photograph in Fig. 13. Here, the construction truck occludes the opposing lane from both the RSU and the ego vehicle, but, thanks to the SR, the ego vehicle can conclude the opposing lane to be free behind the truck. The algorithm remains effective even when several messages are lost or not processed. In the rightmost part of the lane, the ego vehicle has to consider that a possible traffic participant has entered the scene since no free space message in that area has been processed recently.

VII. Conclusion

In this work, we introduce a robust algorithm for incorporating detected free space shared via V2X communication. The standard protocol for CPMs can increase a vehicle's field of view, but, as our experiments show, an occlusion tracking algorithm is necessary to fully benefit from augmented situational awareness. Building on our previous work, we use reachability analysis to sequentially reason about areas possibly occupied by hidden obstacles. In this work, we show how this approach can be extended to safely incorporate delayed messages, making full use of all the available information without solely relying on instantaneous or lossless communication. This was demonstrated in both simulated and real-world experiments featuring challenging, common driving scenarios.

Our work relies on an accurate detection of free space. A natural extension is to include measurement uncertainties and provide a probabilistic estimate of which areas are possibly occupied by hidden obstacles. In this work, we studied a stationary RSU. However, when receiving messages from moving vehicles, state uncertainties may be larger and could introduce measurement errors. In particular, uncertain estimates of a vehicle's heading may lead to large errors when transforming free space measurements to the global frame in which they are communicated. A probabilistic model of hidden obstacles could enable AVs to make informed, risk-aware decisions even in the presence of state uncertainties.

Other possible extensions include more complex vehicle dynamics models, interactions, and traffic rules. This could reduce the overconservativeness of the predictions and provide a more accurate approximation of the true reachable set of states. However, more complex models would also require improvements in computation, such as code optimization and parallelization, as proposed in [24]. Models could also be used to reason about what areas are relevant to track and communicate to others, making better use of the available compute and bandwidth.

Acknowledgment

The authors would like to thank the engineers Petter Wendel, Christer Rickman, Christoffer Norén, Jonny Andersson, Caroline Heidenreich, Samir Kays, and Natalie Richardson at Scania for their support in enabling their real-world experiments. This research has been carried out as a part of the TECoSA Vinnova Competence Center for Trustworthy Edge Computing Systems and Applications at KTH Royal Institute of Technology.

References

[1] Z. Wan et al., "Too afraid to drive: Systematic discovery of semantic DoS vulnerability in autonomous driving planning under physical-world attacks," in *Proc. Netw. Distrib. Syst. Secur. Symp.* Reston, VA, USA: Internet Society, 2022, doi: 10.15607/rss.2021.xvii.066.

[2] J. Condliffe, "Humans will bully mild-mannered autonomous cars," MIT Technology Review, Nov. 2016. [Online]. Available: https://www.technologyreview.com/2016/11/03/156270/humans-will-bully-mild-mannered-autonomous-cars/

[3] A. Shetty, M. Yu, A. Kurzhanskiy, O. Grembek, H. Tavafoghi, and P. Varaiya, "Safety challenges for autonomous vehicles in the absence of connectivity," *Transp. Res. C, Emerg. Technol.*, vol. 128, Jul. 2021, Art. no. 103133.

[4] J. M. G. Sánchez, T. Nyberg, C. Pek, J. Tumova, and M. Törngren, "Foresee the unseen: Sequential reasoning about hidden obstacles for safe driving," in *Proc. IEEE Intell. Vehicles Symp. (IV)*, Jun. 2022, pp. 255–264.

[5] H.-J. Günther, "Collective perception in vehicular ad-hoc networks," Ph.D. dissertation, Inst. Oper. Syst. Comput. Netw., Technische Universität Braunschweig, Braunschweig, Germany, Feb. 2018.

[6] *Road Vehicles—Safety of the Intended Functionality*, Standard ISO 21448:2022, International Organization for Standardization, Geneva, Switzerland, 2022.

[7] *Road Vehicles—Functional Safety*, Standard ISO 26262:2018, International Organization for Standardization, Geneva, Switzerland, Dec. 2018.

[8] G. Fornaro and M. Törngren, "Improving road traffic safety and performance—Barriers and directions towards cooperative automated vehicles," in *Computer Safety, Reliability, and Security. SAFECOMP 2023 Workshops*. Berlin, Germany: Springer-Verlag, Sep. 2023, pp. 283–294.

[9] J. M. G. Sánchez, L. Bruns, J. Tumova, P. Jensfelt, and M. Törngren, "Transitional grid maps: Joint modeling of static and dynamic occupancy," 2024, *arXiv:2401.06518*.

[10] W. Chung et al., "Safe navigation of a mobile robot considering visibility of environment," *IEEE Trans. Ind. Electron.*, vol. 56, no. 10, pp. 3941–3950, Oct. 2009.

[11] S. Bouraine, T. Fraichard, and H. Salhi, "Provably safe navigation for mobile robots with limited field-of-views in unknown dynamic environments," in *Proc. IEEE Int. Conf. Robot. Autom.*, May 2012, pp. 174–179.

[12] M. Lee, K. Jo, and M. Sunwoo, "Collision risk assessment for possible collision vehicle in occluded area based on precise map," in *Proc. IEEE 20th Int. Conf. Intell. Transp. Syst. (ITSC)*, Oct. 2017, pp. 1–6.

[13] M.-Y. Yu, R. Vasudevan, and M. Johnson-Roberson, "Occlusion-aware risk assessment for autonomous driving in urban environments," *IEEE Robot. Autom. Lett.*, vol. 4, no. 2, pp. 2235–2241, Apr. 2019.

[14] Z. Zhang and J. Fisac, "Safe occlusion-aware autonomous driving via game-theoretic active perception," in *Proc. Robot., Sci. Syst. XVII*, Jul. 2021, doi: 10.14722/ndss.2022.24177.

[15] S. Brechtel, T. Gindele, and R. Dillmann, "Probabilistic decision-making under uncertainty for autonomous driving using continuous POMDPs," in *Proc. 17th Int. IEEE Conf. Intell. Transp. Syst. (ITSC)*, Oct. 2014, pp. 392–399.

[16] P. Schörner, L. Töttel, J. Doll, and J. M. Zöllner, "Predictive trajectory planning in situations with hidden road users using partially observable Markov decision processes," in *Proc. IEEE Intell. Vehicles Symp. (IV)*, Jun. 2019, pp. 2299–2306.

[17] M. Althoff and S. Magdici, "Set-based prediction of traffic participants on arbitrary road networks," *IEEE Trans. Intell. Vehicles*, vol. 1, no. 2, pp. 187–202, Jun. 2016.

[18] M. Koschi and M. Althoff, "SPOT: A tool for set-based prediction of traffic participants," in *Proc. IEEE Intell. Vehicles Symp. (IV)*, Jun. 2017, pp. 1686–1693.

[19] M. Koschi, C. Pek, M. Beikirch, and M. Althoff, "Set-based prediction of pedestrians in urban environments considering formalized traffic rules," in *Proc. 21st Int. Conf. Intell. Transp. Syst. (ITSC)*, Nov. 2018, pp. 2704–2711.

[20] P. F. Orzechowski, A. Meyer, and M. Lauer, "Tackling occlusions & limited sensor range with set-based safety verification," in *Proc. 21st Int. Conf. Intell. Transp. Syst. (ITSC)*, Nov. 2018, pp. 1729–1736.

[21] M. Koschi and M. Althoff, "Set-based prediction of traffic participants considering occlusions and traffic rules," *IEEE Trans. Intell. Vehicles*, vol. 6, no. 2, pp. 249–265, Jun. 2021.

[22] Y. Nager, A. Censi, and E. Frazzoli, "What lies in the shadows? Safe and computation-aware motion planning for autonomous vehicles using intent-aware dynamic shadow regions," in *Proc. Int. Conf. Robot. Automat. (ICRA)*, 2019, pp. 5800–5806.

[23] L. Wang, C. Burger, and C. Stiller, "Reasoning about potential hidden traffic participants by tracking occluded areas," in *Proc. IEEE Int. Intell. Transp. Syst. Conf. (ITSC)*, Sep. 2021, pp. 157–163.

[24] T. Nyberg, J. van Haastregt, and J. Tumova, "Highway-driving with safe velocity bounds on occluded traffic," in *Proc. IEEE Int. Conf. Robot. Autom. (ICRA)*, May 2024, pp. 6828–6835.

[25] Y. Han, H. Zhang, H. Li, Y. Jin, C. Lang, and Y. Li, "Collaborative perception in autonomous driving: Methods, datasets, and challenges," *IEEE Intell. Transp. Syst. Mag.*, vol. 15, no. 6, pp. 131–151, Nov. 2023.

[26] S. Hu, Z. Fang, Y. Deng, X. Chen, and Y. Fang, "Collaborative perception for connected and autonomous driving: Challenges, possible solutions and opportunities," 2024, *arXiv:2401.01544*.

[27] *Intelligent Transport Systems (ITS); Vehicular Communications; Basic Set of Applications; Analysis of the Collective Perception Service (CPS)*, Standard ETSI TR 103 562, Version 2.1.1, European Telecommunications Standards Institute, Dec. 2019.

[28] *Intelligent Transport Systems (ITS); ITS-G5 Access Layer Specification for Intelligent Transport Systems Operating in the 5 GHz Frequency Band*, Standard ETSI en 302 663, Version 1.3.1, European Telecommunications Standards Institute, Jan. 2020.

[29] M. Hasan, S. Mohan, T. Shimizu, and H. Lu, "Securing vehicle-to-everything (V2X) communication platforms," *IEEE Trans. Intell. Vehicles*, vol. 5, no. 4, pp. 693–713, Dec. 2020.

[30] J. Wang, Y. Shao, Y. Ge, and R. Yu, "A survey of vehicle to everything (V2X) testing," *Sensors*, vol. 19, no. 2, p. 334, Jan. 2019.

[31] V. Narri, A. Alanwar, J. Mårtensson, C. Norén, L. D. Col, and K. H. Johansson, "Set-membership estimation in shared situational awareness for automated vehicles in occluded scenarios," in *Proc. IEEE Intell. Vehicles Symp. (IV)*, Jul. 2021, pp. 385–392.

[32] V. Narri, A. Alanwar, J. Mårtensson, C. Norén, and K. H. Johansson, "Shared situational awareness with V2X communication and set-membership estimation," 2023, *arXiv:2302.05224*.

[33] M. Buchholz et al., "Handling occlusions in automated driving using a multiaccess edge computing server-based environment model from infrastructure sensors," *IEEE Intell. Transp. Syst. Mag.*, vol. 14, no. 3, pp. 106–120, May 2022.

[34] J. Müller, J. Strohbeck, M. Herrmann, and M. Buchholz, "Motion planning for connected automated vehicles at occluded intersections with infrastructure sensors," *IEEE Trans. Intell. Transp. Syst.*, vol. 23, no. 10, pp. 17479–17490, Oct. 2022.

[35] S. Li, K. Shu, C. Chen, and D. Cao, "Planning and decision-making for connected autonomous vehicles at road intersections: A review," *Chin. J. Mech. Eng.*, vol. 34, no. 1, p. 133, Dec. 2021.

[36] C. Zhang, F. Steinhauser, G. Hinz, and A. Knoll, "Occlusion-aware planning for autonomous driving with vehicle-to-everything communication," *IEEE Trans. Intell. Vehicles*, vol. 9, no. 1, pp. 1229–1242, Jan. 2024.

[37] B. Chazelle, "The polygon containment problem," *Adv. Comput. Res.*, vol. 1, no. 1, pp. 1–33, 1983.

[38] S. Lefèvre, D. Vasquez, and C. Laugier, "A survey on motion prediction and risk assessment for intelligent vehicles," *ROBOMECH J.*, vol. 1, no. 1, pp. 1–14, Dec. 2014.

[39] M. Gulzar, Y. Muhammad, and N. Muhammad, "A survey on motion prediction of pedestrians and vehicles for autonomous driving," *IEEE Access*, vol. 9, pp. 137957–137969, 2021.

[40] M. Althoff, M. Koschi, and S. Manzinger, "CommonRoad: Composable benchmarks for motion planning on roads," in *Proc. IEEE Intell. Veh. Symp.*, Jun. 2017, pp. 719–726.

[41] C. Pek, V. Rusinov, S. Manzinger, M. C. Üste, and M. Althoff, "CommonRoad drivability checker: Simplifying the development and validation of motion planning algorithms," in *Proc. IEEE Intell. Vehicles Symp.*, Oct. 2020, pp. 1013–1020.

[42] S. Gillies et al., "Shapely: Manipulation and analysis of geometric objects," 2007. [Online]. Available: https://pypi.org/project/shapely/1.8.0/

[43] A. Rauch, F. Klanner, and K. Dietmayer, "Analysis of V2X communication parameters for the development of a fusion architecture for cooperative perception systems," in *Proc. IEEE Intell. Vehicles Symp. (IV)*, Jun. 2011, pp. 685–690.

Truls Nyberg (Member, IEEE) received the M.Sc. degree in engineering applied physics and electrical engineering from Linköping University, Linköping, Sweden, in 2018, specializing in control and information systems. He is currently pursuing the Ph.D. degree with Scania CV AB, Södertälje, Sweden, and the Division of Robotics, Perception, and Learning, KTH Royal Institute of Technology, Stockholm, Sweden, with partial support from the Wallenberg AI, Autonomous Systems, and Software Program (WASP) funded by the Knut and Alice Wallenberg Foundation.

As part of his studies, he completed a research visit at the Autonomous Vehicle Systems (AVS) Laboratory, Technical University of Munich, Munich, Germany. His research focuses on risk-aware decision-making and situational awareness for autonomous vehicles, with an emphasis on applications for heavy-duty trucks and buses.

José Manuel Gaspar Sánchez received the M.Sc. degree in industrial engineering from the University of Málaga, Málaga, Spain, in 2018. He is currently pursuing the Ph.D. degree with the Division of Mechatronics and Embedded Control Systems, KTH Royal Institute of Technology, Stockholm, Sweden.

He is also a Visiting Student Researcher with Stanford Intelligent Systems Laboratory (SISL), Stanford University, Stanford, CA, USA. His research focuses on enhancing situational awareness for autonomous agents with limited sensing capabilities. His research interests include Bayesian networks and reachability analysis, with a particular emphasis on their applications in perception and tracking.

Vandana Narri (Graduate Student Member, IEEE) received the M.Sc. degree in electrical engineering with a specialization in signal processing from the Blekinge Institute of Technology, Karlskrona, Sweden, in 2017. She is currently pursuing the Ph.D. degree with Scania CV AB, Södertälje, Sweden, and the Division of Decision and Control Systems, KTH Royal Institute of Technology, Stockholm, Sweden.

Her research aims to enhance situational awareness of heavy-duty vehicles in complex urban environments using vehicular communication and set-based methods. Her work is partially supported by the Wallenberg Artificial Intelligence, Autonomous Systems, and Software Program (WASP) funded by the Knut and Alice Wallenberg Foundation.

Henrik Pettersson received the M.Sc. and Ph.D. degrees from the Division of Fluid and Mechanical Engineering Systems, Department of Mechanical Engineering, Linköping University, Linköping, Sweden, in 1995 and 2002, respectively.

He began working for Scania CV AB, Södertälje, Sweden, in 2002, focusing on the development of powertrain control systems, where he is currently a Senior Technical Advisor with the Autonomous Transport Solutions Department. Since 2010, he has been working in predevelopment and research, concentrating on fuel-saving functionality for heavy-duty vehicles based on cooperative driving and V2X communication, such as platooning. Since 2016, his focus has shifted to autonomous vehicles.

Jonas Mårtensson (Member, IEEE) received the M.Sc. degree in vehicle engineering and the Ph.D. degree in automatic control from the KTH Royal Institute of Technology, Stockholm, Sweden, in 2002 and 2007, respectively.

He is currently a Professor with the Division of Decision and Control Systems, KTH Royal Institute of Technology, where he also serves as the Director of the Integrated Transport Research Laboratory (ITRL), a multidisciplinary research center focused on sustainable transport systems in collaboration with Swedish industry and public stakeholders. His research interests span efficient and sustainable transport systems, including cooperative traffic control and control of connected and automated vehicles, with a particular interest in freight and heavy vehicles.

Dr. Mårtensson received the title of Docent in 2016.

Karl H. Johansson (Fellow, IEEE) received the M.Sc. degree in electrical engineering and the Ph.D. degree in automatic control from Lund University, Lund, Sweden, in 1992 and 1997, respectively.

He has held visiting positions at UC Berkeley, Berkeley, CA, USA; Caltech, Pasadena, CA, USA; NTU, Singapore; and other prestigious institutions. He is currently a Swedish Research Council Distinguished Professor of electrical engineering and computer science with the KTH Royal Institute of Technology, Stockholm, Sweden, and the Founding Director of Digital Futures, Stockholm. His research focuses on networked control systems and cyber–physical systems, with applications in transportation, energy, and automation networks.

Dr. Johansson has been a member of the Swedish Scientific Council for Natural Sciences and Engineering Sciences. He is a fellow of the Royal Swedish Academy of Engineering Sciences. For his scientific contributions, he received numerous best paper awards and distinctions from IEEE, IFAC, and other organizations. He has been recognized as a Distinguished Professor by the Swedish Research Council, a Wallenberg Scholar by the Knut and Alice Wallenberg Foundation, and a Future Research Leader by the Swedish Foundation for Strategic Research. He also received the Triennial IFAC Young Author Prize and the IEEE CSS Distinguished Lecturer Award. He was a recipient of the 2024 IEEE CSS Hendrik W. Bode Lecture Prize. His extensive service to the academic community includes roles as the President of the European Control Association, the IEEE CSS Vice President for Diversity, Outreach, and Development, and a member of the IEEE CSS Board of Governors and IFAC Council. He has served on the editorial boards of *Automatica*, IEEE TRANSACTIONS ON AUTOMATIC CONTROL, IEEE TRANSACTIONS ON CONTROL OF NETWORK SYSTEMS, and many other journals.

Martin Törngren (Senior Member, IEEE) received the Ph.D. degree in mechatronics from the KTH Royal Institute of Technology, Stockholm, Sweden, in 1995.

Since 2002, he has been a Professor of embedded control systems with the Division of Mechatronics and Embedded Control Systems, KTH. A pioneer in bridging the fields of automatic control and real-time distributed systems, his recent research has focused on architectural design and the safety of autonomous, trustworthy cyber–physical systems. He has spent several periods abroad as a Visiting Scholar, including time at the University of California at Berkeley, Berkeley, CA, USA, and the Stevens Institute of Technology, Hoboken, NJ, USA. Throughout his career, networking and multidisciplinary research have been central themes. He established the Innovative Center for Embedded Systems, a KTH-industry competence network, in 2008. He is currently the Director of the Swedish Research Center on Trustworthy Edge Computing Systems and Applications, Stockholm.

Jana Tumova (Member, IEEE) received the Ph.D. degree in computer science from Masaryk University, Brno, Czechia, in 2013.

She has been a Visiting Researcher with MIT, Cambridge, MA, USA; Boston University, Boston, MA, USA; and the Singapore-MIT Alliance, Singapore. She is currently an Associate Professor with the Division of Robotics, Perception and Learning, KTH Royal Institute of Technology, Stockholm, Sweden. Her research interests include formal methods for decision-making, motion planning, and control in autonomous systems.

Dr. Tumova received an ACCESS Postdoctoral Fellowship at KTH in 2013. She was a recipient of the Swedish Research Council Starting Grant and the Early Career Award from the Robotics: Science and Systems Foundation.